COMPARISON OF STRUCTURED AND UNSTRUCTURED MESH FOR NUMERICAL SIMULATION OF TURBULENT FLOW AROUND S809 AIRFOIL

Gabriel Victor Costa Pereira [(1)] (gbrielcsta@aluno.ufsj.edu.br), Rafael Romão da Silva Melo [(2)] (rafaelmelo@ufsj.edu.br)

[(1)] Federal University of Sao Joao del-Rei (UFSJ); Dep. of Thermal Science and Fluids

ABSTRACT: In this study, turbulent flow computations were performed on structured and unstructured meshes around the S809 airfoil. The objectives are to assess the mesh reliability for some turbulent models for numerical validation. The numerical simulations were performed an open-source computational fluid dynamics (CFD) platform code based on the Field Operation and Manipulation C++ class library for continuum mechanics (OpenFOAM). First, the turbulent flow is modeled using an unsteady incompressible Reynolds Averaged Navier-Stokes solver. Moreover, CFD computations were realized to study mesh dependency and computational cost in detail. To validate the results, comparisons of the computed aerodynamic coefficients were made with wind tunnel data from the Delft University of Technology (DUT). Finally, ways to improve the reliability of structured and unstructured meshes are discussed by comparing the results. The results show good agreement between simulations and experiments, with the structured mesh showing less error compared to the unstructured mesh.

KEYWORDS: *CFD, Structured Mesh, Unstructured Mesh, Airfoil, S809*

RESPONSIBILITY NOTICE

The authors are solely responsible for this work.

1. INTRODUCTION

In recent years, with the growth of the world economy, wind energy has gained a lot of strength, and today, in Brazil, it represents more than 10% of the country's electricity matrix. From a clean and renewable source, the expansion of wind energy brings numerous environmental benefits. For greater ease of expansion, we can resort to numerical simulations, because with them it is possible to enhance the implementation and production process and contribute to reducing wind turbine design time.

In computational fluid dynamics (CFD), due to the absence of automation techniques, mesh generation is an artisanal process. The numerical solution of turbulent flow around airfoils depends on the level of refinement at some points in the mesh. However, the use of a very refined and complex mesh can lead to a high computational cost without a significant difference in the final result.

In this context, it is proposed to discuss in this work simulations of turbulent flow in structured and unstructured mesh in order to verify the reliability of the meshes for different levels of refinement and turbulence models. Since the numerical solutions must express good consistency with the experimental data presented by Jonkman (2003).

2. THE S809 AIRFOIL

This study performed two-dimensional turbulent flow computations on structured and unstructured meshes around the S809 airfoil (Figure 1).

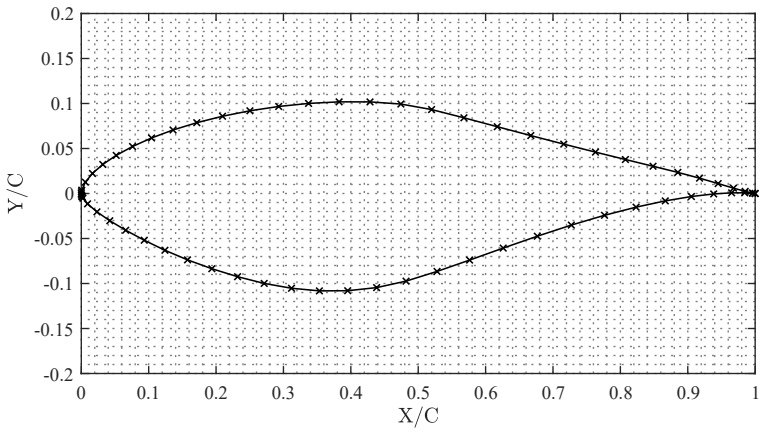

FIGURE 1. S809 airfoil. Font: Authors (2022).

The computations were analyzed using the URANS approach and some turbulent models implemented in the open-source computational fluid dynamics platform – OpenFOAM. The

objectives of this work are to assess the mesh reliability to validate the applied numerical methods based on good-quality experimental data. In addition, such detailed comparative works between different types of meshes around airfoils were not found, making the present work a contribution.

In this paper, the comparison of aerodynamic coefficients of the airfoil is presented at Reynolds number of 1×10^6 for two types of meshes: structured and unstructured. Due the analyzes are detailed and very time-consuming, these aerodynamic coefficients were analyzed for ten different angles of attack, α: $-1.04°$, $0°$, $1.02°$, $4.10°$, $6.16°$, $8.20°$, $10.20°$, $12.23°$, $15.23°$, $17.21°$.

3. NUMERICAL PROCEDURE

3.1. Turbulence Modeling

The open-source CFD code, OpenFOAM, contains a wide variety of turbulence models to build the numerical simulation. In this research, there are three implemented turbulence models to compare results: Spalart-Allmaras (S-A), SST k/ω, and Standard k/ϵ. For all turbulence models, it is important to note that the constant values of the equations are detailed in their main references.

3.1.1. Sparlart-Allmaras (S-A) model

The turbulence closure model proposed by Spalart and Allmaras (1992) is a one-equation model with which it is possible to solve a modeled balance equation for the kinematic eddy turbulent viscosity. The dynamic turbulent viscosity μ_t is determined by the modified turbulent viscosity $\tilde{\nu}$ and damped by the function f_{v1} near the walls:

$$\mu_t = \rho \tilde{\nu} f_{v1}, \tag{1}$$

where f_{v1} is

$$f_{v1} = \frac{\chi^3}{\chi^3 + C_{v1}^3}, \tag{2}$$

and

$$\chi = \frac{\tilde{\nu}}{\nu}. \tag{3}$$

The variable $\tilde{\nu}$ is solved using the following equation:

$$\frac{\partial \tilde{\nu}}{\partial t} + \bar{u_j}\frac{\partial \tilde{\nu}}{\partial x_j} = \frac{1}{\sigma}\left[\frac{\partial}{\partial x_j}\left((\nu + \tilde{\nu})\frac{\partial}{\partial x_j}\tilde{\nu}\right) + C_{b2}|\nabla\tilde{\nu}|^2\right] + C_{b1}\tilde{S}\tilde{\nu} - C_{w1}f_w\left(\frac{\tilde{\nu}}{d}\right)^2. \quad (4)$$

The term $\tilde{S}$ is composed by the sum of the strain-rate tensor S and a damping function which actuates near the walls, through the function f_{v2}

$$\tilde{S} \equiv S + \frac{\tilde{\nu}}{\kappa^2 d^2} f_{v2}, \quad (5)$$

where

$$f_{v2} = 1 - \frac{\chi}{1 + \chi f_{v1}}, \quad (6)$$

and d is the distance for the nearest wall. S is determined by:

$$S = \sqrt{2\Omega_{ij}\Omega_{ij}}, \quad (7)$$

where Ω_{ij} is the anti-symmetric component of the velocity gradient:

$$\Omega_{ij} = \frac{1}{2}\left(\frac{\partial u_i}{\partial x_j} - \frac{\partial u_j}{\partial x_i}\right). \quad (8)$$

The function f_w is defined as unitary in the logarithmic region of the boundary layer, as follow,

$$f_w = g\left(\frac{1 + C_{w3}^6}{g^6 + C_{w3}^6}\right)^{1/6}, \quad (9)$$

where

$$g = r + C_{w2}(r^6 - r), \quad (10)$$

and

$$r \equiv \frac{\tilde{\nu}}{\tilde{S}\kappa^2 d^2}. \tag{11}$$

Additionally, the constants of the model were empirically determined, which are the following: $\sigma = 2/3$; $C_{b1} = 0.1355$; $C_{b2} = 0.622$; $\kappa = 0.41$; $C_{w1} = C_{b1}/\kappa^2 + (1 + C_{b2})/\sigma$; $C_{w2} = 0.3$; $C_{w3} = 2$; $C_{v1} = 7.1$.

3.1.2. Standard k/ϵ model

The Standard k/ϵ model, proposed by Launder and Spalding (1972) is the URANS turbulence closure model the in the present work. Two additional balance equations need to be solved. The transport of turbulent kinetic energy, k $[\mathrm{m^2/s^2}]$, is modeled using the following balance equation:

$$\rho\frac{\partial k}{\partial t} + \rho u_i \frac{\partial k}{\partial x_i} = \frac{\partial}{\partial x_i}\left[\left(\mu + \frac{\mu_t}{\sigma_k}\right)\frac{\partial k}{\partial x_i}\right] + \mu_t S^2 - \rho\epsilon, \tag{12}$$

where ρ is the specific mass of the fluid, μ and μ_t are the molecular and the turbulent dynamic viscosity, respectively, $\sigma_k = 1.0$ is the model constant and $S = \sqrt{S_{ij}S_{ij}}$, in which S_{ij} represents the strain rate tensor components.

The balance of specific power of turbulent kinetic energy transformation, ϵ $[\mathrm{m^2/s^3}]$, is modeled using the equation:

$$\rho\frac{\partial \epsilon}{\partial t} + \rho u_i \frac{\partial \epsilon}{\partial x_i} = \frac{\partial}{\partial x_i}\left[\left(\mu + \frac{\mu_t}{\sigma_\epsilon}\right)\frac{\partial \epsilon}{\partial x_i}\right] + C_{\epsilon 1}\frac{\epsilon}{k}\mu_t S^2 - \rho C_{\epsilon 2}\frac{\epsilon^2}{k} \tag{13}$$

where $\sigma_\epsilon = 1.3$, $C_{\epsilon 1} = 1.44$ e $C_{\epsilon 2} = 1.92$ are the model constants.

And the turbulent viscosity is calculated using Equation 14:

$$\nu_t = C_\mu \frac{k^2}{\epsilon} \tag{14}$$

where $C_\mu = 0.09$.

When is desired to simulate wall flows using the standard k/ϵ model, an additional model is required for near-wall regions. In the present work, the standard wall treatment was used.

3.1.3. SST k/ω model

The SST turbulence closure contains two blending functions, F_1 and F_2, which bridge the near-wall k/ω formulation with the away-from-wall k/ϵ formulation. The SST is expressed in terms of k and ω.

It is necessary to calculate the turbulent kinetic energy k and the Kolmogorov frequency scale ω for calculate the turbulent viscosity, through a balance equation, for each of these variables. The balance equation for k and ω in the SST model (Menter et al., 2003) are, respectively:

$$\rho\frac{\partial k}{\partial t}+\rho\overline{u_j}\frac{\partial k}{\partial x_j}=P_k-\beta^*\rho k\omega+\frac{\partial}{\partial x_j}\left[(\mu+\sigma_k\mu_t)\frac{\partial k}{\partial x_j}\right], \tag{15}$$

$$\rho\frac{\partial \omega}{\partial t}+\rho\overline{u_j}\frac{\partial \omega}{\partial x_j}=\alpha\rho S^2-\beta\rho\omega^2+\frac{\partial}{\partial x_j}\left[(\mu+\sigma_\omega\mu_t)\frac{\partial \omega}{\partial x_j}\right]+2(1-F_1)\sigma_{\omega2}\frac{\rho}{\omega}\frac{\partial k}{\partial x_i}\frac{\partial \omega}{\partial x_i}, \tag{16}$$

where,

$$P_k=\min\left(\rho\tau_{ij}\frac{\partial\overline{u_i}}{\partial x_j},10\beta^*\rho k\omega\right). \tag{17}$$

The blending function F_1 is calculated using the equation:

$$F_1=\tanh\left\{\left\{\min\left[\max\left(\frac{\sqrt{k}}{\beta^*\omega y},\frac{500\nu}{y^2\omega}\right),\frac{4\sigma_{\omega2}k}{CD_{k\omega}y^2}\right]\right\}^4\right\}, \tag{18}$$

where,

$$CD_{k\omega}=\max\left(2\rho\sigma_{\omega2}\frac{1}{\omega}\frac{\partial k}{\partial x_i}\frac{\partial \omega}{\partial x_i},10^{-10}\right). \tag{19}$$

In the SST model, the kinematic turbulent viscosity is given by:

$$\nu_T = \frac{a_1 k}{\max(a_1 \omega, SF_2)}, \tag{20}$$

and the second blending function F_2 is calculated as follow:

$$F_2 = \tanh\left\{\left[\max\left(\frac{2\sqrt{k}}{\beta^* \omega y}, \frac{500\nu}{y^2 \omega}\right)\right\}^2\right]. \tag{21}$$

The constants used in the transport equations for k and ω are weighted by the mixing function F_1, through the following generic equation:

$$\phi = \phi_1 F_1 + \phi_2 (1 - F_1). \tag{22}$$

Additionally, the constants of the model are: $\alpha_1 = 5/9$, $\alpha_2 = 0.44$, $\beta_1 = 3/40$, $\beta_2 = 0.0828$, $\beta^* = 9/100$, $\sigma_{k1} = 0.85$, $\sigma_{k2} = 1$, $\sigma_{\omega 1} = 0.5$ and $\sigma_{\omega 2} = 0.856$.

3.2. Computational domain

For structured and unstructured meshes, the computational fluid domain, illustrated in Figure 2, was decided to be semi-circular. The domain extends 25 chord lengths after the trailing edge and the radius of the semicircle is 15 chords. Two types of boundary conditions were selected for numerical analyses: velocity inlet and pressure outlet. In addition, it is considered a plane of symmetry on the sides of the domain.

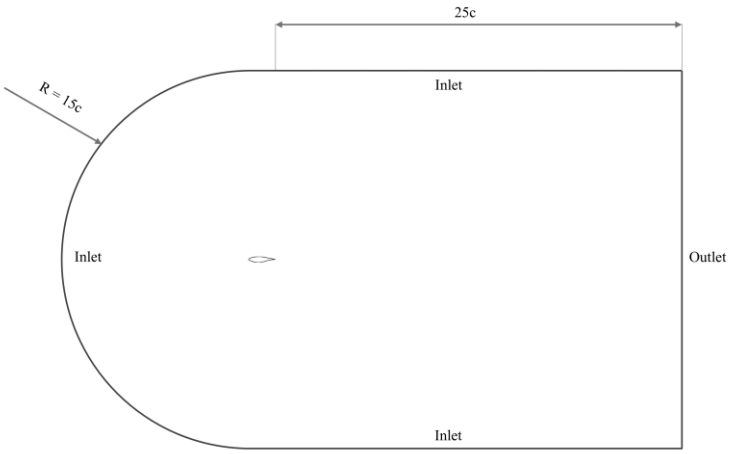

FIGURE 2. Semi-circular domain. Font: Authors (2022).

In the time of simulation, the incidence of the airfoil with respect to the computing domain was not changed. Thus, the coefficients in aerodynamic axis can be obtained by the expressions:

$$C_L = C_Y \cos\alpha - C_X \sin\alpha \tag{23}$$

and

$$C_D = C_Y \sin\alpha + C_X \cos\alpha, \tag{24}$$

where C_X and C_Y represents the aerodynamic coefficients components in the lift coefficient, C_L, and drag coefficient, C_D, relative to the angle of attack, α.

3.3. Computational mesh

To simulate the airfoil, structured and unstructured meshes were performed. According to Çengel and Cimbala (2010), for greater ease of solution of the boundary layer, the meshes were refined around the airfoil with greater resolution in the leading and trailing edges and the wake region.

The selected meshes came as the results of a mesh dependence study, conducted for structured and unstructured meshing configurations. The mesh dependency study was very important to this work, serving to compare aerodynamic coefficients us three turbulence models for low, mid, and high angles of attack, α. The results obtained from the dependency study can be visualized in Figures 3, 4 and 5.

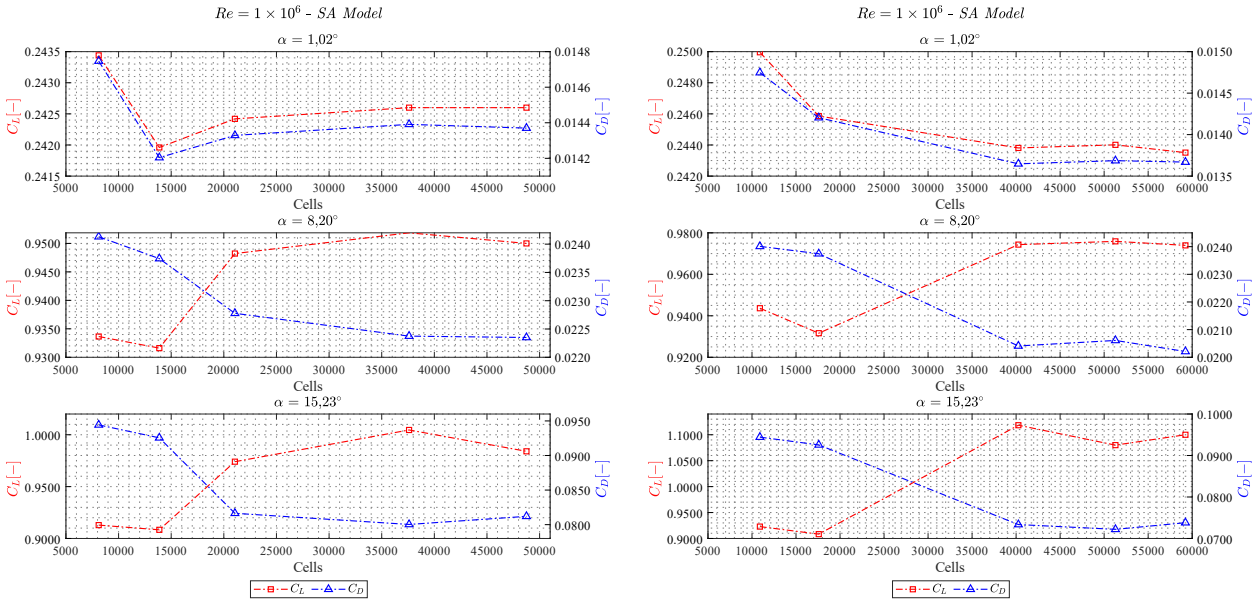

(a) (b)

FIGURE 3. Results of the S-A Model for (a) structured and (b) unstructured meshes.

Font: Authors (2022).

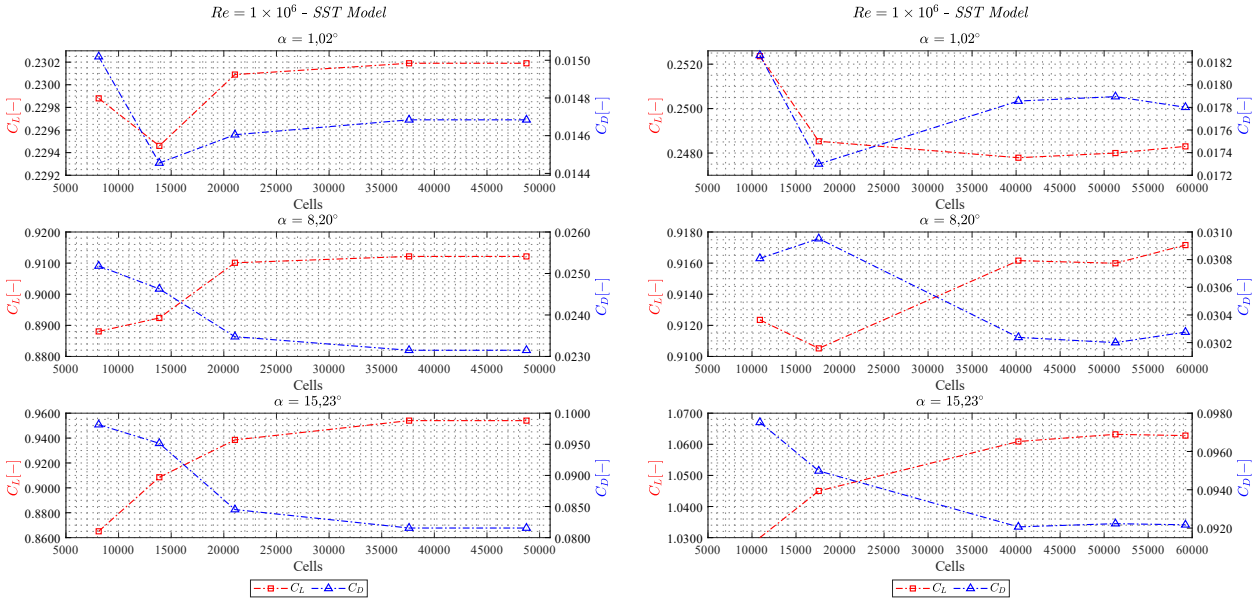

(a) (b)

FIGURE 4. Results of the SST k/ω Model for (a) structured and (b) unstructured meshes.

Font: Authors (2022).

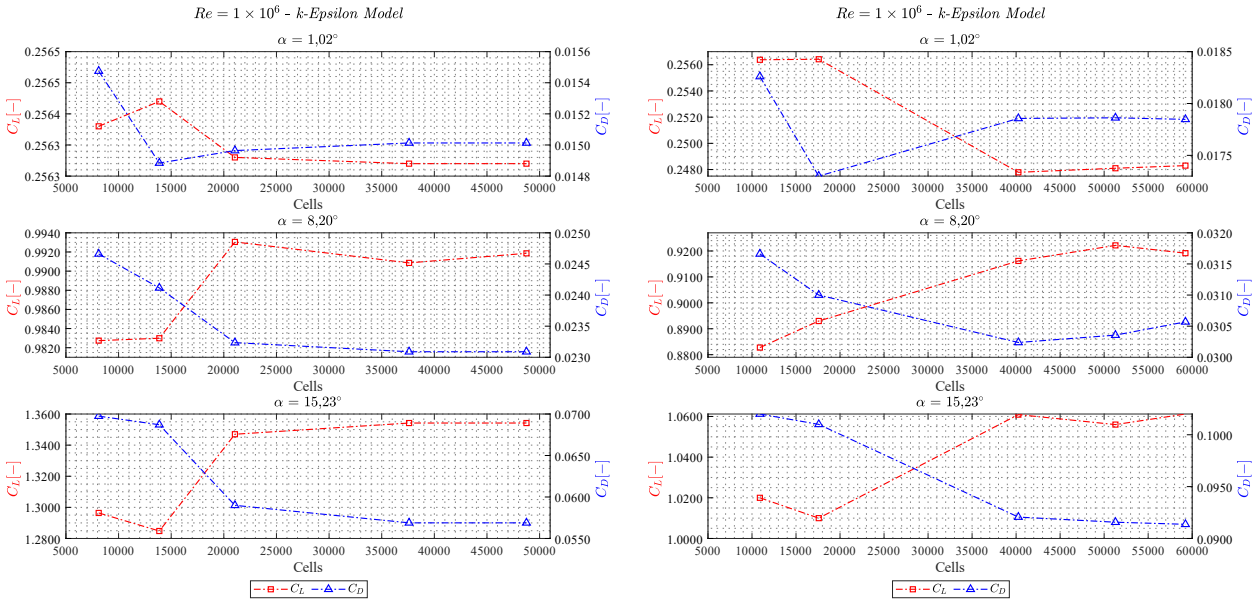

(a) (b)

FIGURE 5. Results of the Standard k/ϵ Model for (a) structured and (b) unstructured meshes. Font: Authors (2022).

In addition, it was evaluated the y^+ variation in function of all created meshes (Figure 6).

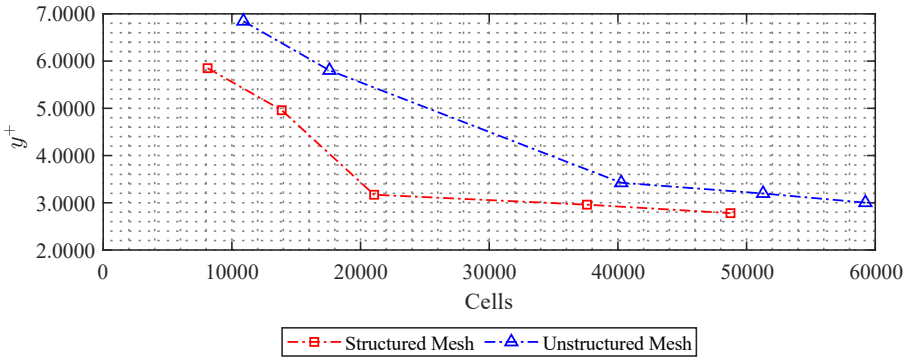

FIGURE 6. Variation of y^+ in relation to the number of cells. Font: Authors (2022).

We observed that a structured grid with 21000 cells provides good results for all turbulence models. For unstructured meshes, satisfactory results were obtained for 40000 cells. Therefore, these meshes presented reliable results for the continuity of the numerical simulations. Figure 7 show the structured and unstructured meshes.

The advantage of this approach was that, compared to the experimental data, satisfactory results were obtained without increasing the computational cost in meshes of higher resolution.

Proof of this are the values of y^+ that were between 3 and 6 for the two meshes, sufficient size to properly resolve the inner parts of the boundary layer, according to Fleck et al. (2014) and Salim and Cheah (2009).

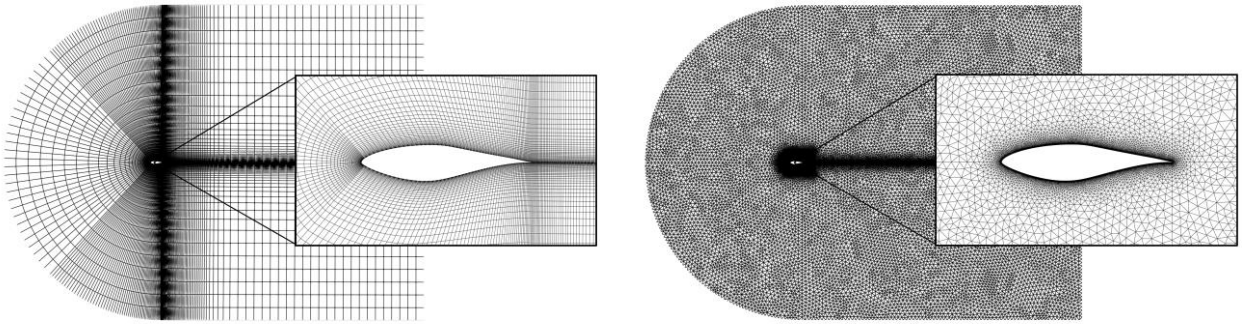

(a) (b)

FIGURE 7. Selected (a) structured and (b) unstructured meshes.
Font: Authors (2022).

3.4. Boundary conditions

Firstly, the inlet boundary condition is applied to the free stream velocity and turbulence quantities. The pressure outlet boundary condition defines an outflow condition based on the flow pressure (p) at the outlet. On the airfoil surface, the no-slip condition is imposed on the velocity components.

The hypothesis of steady state was considered in the analysis, with the fluid considered incompressible and without temperature variations. The temperature was chosen to be the same as the environmental temperature, $T = 300\ K$. Then, the density of the air is $\rho = 1.225\ \mathrm{kg/m^3}$ and the viscosity is $\mu = 1.7894 \times 10^{-5}\ \mathrm{kg/ms}$. The prescribed module velocity at the inlet is $U_\infty = 14.607\ \mathrm{m/s}$ corresponding a Reynolds number of 1×10^6. To change the angle of attack, α, the X component, U_x, and Y component, U_y, of the velocity vector were varied obtaining the relation

$$U_\infty = \sqrt{U_x^2 + U_y^2} \tag{25}$$

For SST k/ω and Standard k/ϵ models, the free-stream turbulent energy and the dissipation rate of turbulent energy are calculed by the expressions:

$$k = \frac{3}{2}(U_\infty \cdot I)^2 \tag{26}$$

and

$$\omega = \frac{k^{0.5}}{C_\mu^{0.25} L}, \qquad \epsilon = \frac{C_\mu^{0.75} k^{1.5}}{L}, \tag{27}$$

where $I = 0.01\%$ is the turbulence intensity and reference length scale, L, is equal to $1\ \mathrm{m}$.

Furthermore, were used the SIMPLE (Semi-Implicit Method for Pressure Linked Equations) for solve pressure-velocity coupling equations, for the discretization method, were used the linear upwind scheme, both standard algorithms in OpenFOAM. For the convergence criteria from absolute residuals of all equations, variables are set below 10^{-5}.

4. RESULTS AND DISCUSSIONS

The computational results are compared to the experimental data obtained by Ohio State University (OSU) and the Delft University of Technology (DUT) (Jonkman, 2003). The experimental results exposed herein were obtained with free transition and a Reynolds number of 1×10^6.

4.1. Lift and drag coefficients

The lift and drag coefficients were possible to be predicted employing the presented turbulence models, and then be examined and compared with reliable experimental data.

Figures 8 and 9 illustrate the simulation results of the lift and drag coefficients for the S809 airfoil versus the angle of attack, α.

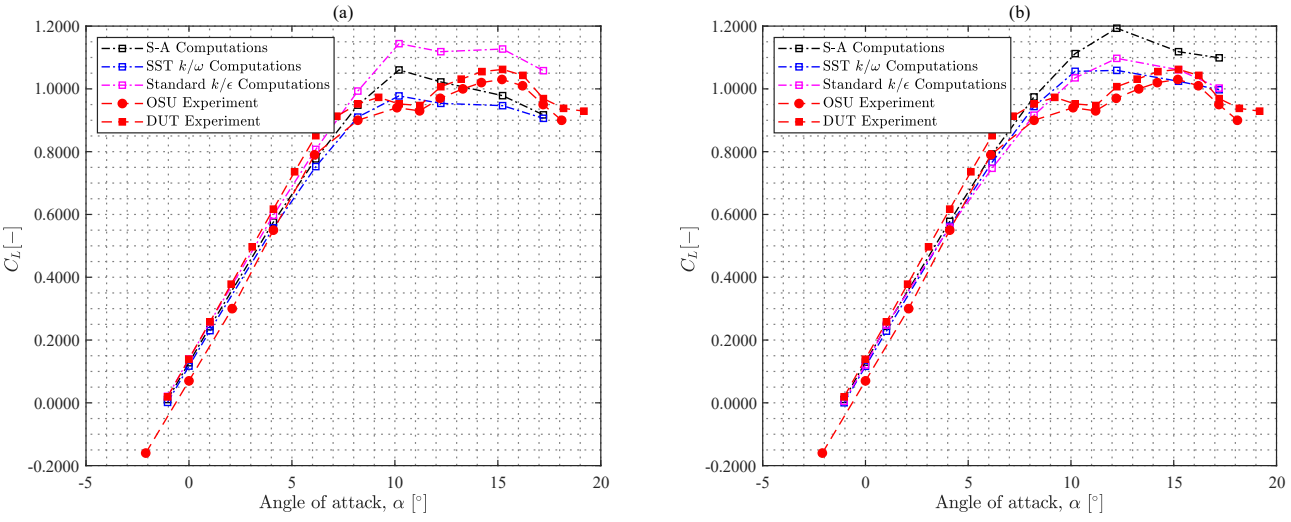

FIGURE 8. Comparison between experimental data and computational results of the lift coefficient curve for (a) structured mesh and (b) unstructured mesh at Reynolds number of 1×10^6. Font: Authors (2022).

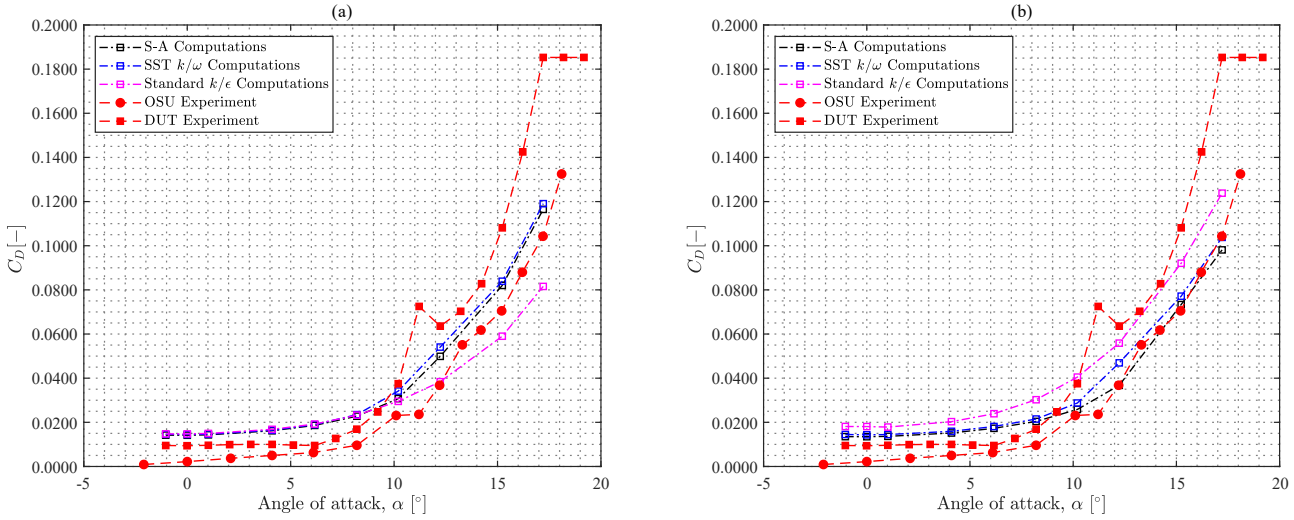

FIGURE 9. Comparison between experimental data and computational results of the lift coefficient curve for (a) structured mesh and (b) unstructured mesh at Reynolds number of 1×10^6. Font: Authors (2022).

The prediction of lift coefficients showed good agreement with the experimental results in all meshes and turbulence models. All models presented difficulty in converging at high angles of attack, which may be due to the imprecise value of the free-flow turbulence intensity. However, for the stall region that is between the $\alpha = 10.20°$ to $11.21°$, a better C_L prediction of the structured mesh was observed with the SST k/ω model. In addition, it is worth mentioning that the unstructured mesh also presented good results in the stall region with the SST k/ω model, but with a greater error about structured mesh results. These results confirm the performance of the SST k/ω model for modeling turbulent flow around airfoils.

The variation of the drag coefficient with the angle of attack also showed good agreement between the Spalart-Allmaras and SST k/ω models with the experiments for $\alpha \leq 15.23°$, in both meshes. However, the unstructured mesh presented a lower error concerning the experiment performed by Ohio State University (Jonkman, 2003), while the structured mesh presented errors similar to the two experiments.

4.2. Contours

Figures 10, 11, 12, 13, 14 and 15 present the region around S809 airfoil using contours of velocity, static pressure and turbulent viscosity for $\alpha = 4.10°$ and $15.23°$, at Reynolds number of 1×10^6 with S-A, SST k/ω and Standard k/ϵ models.

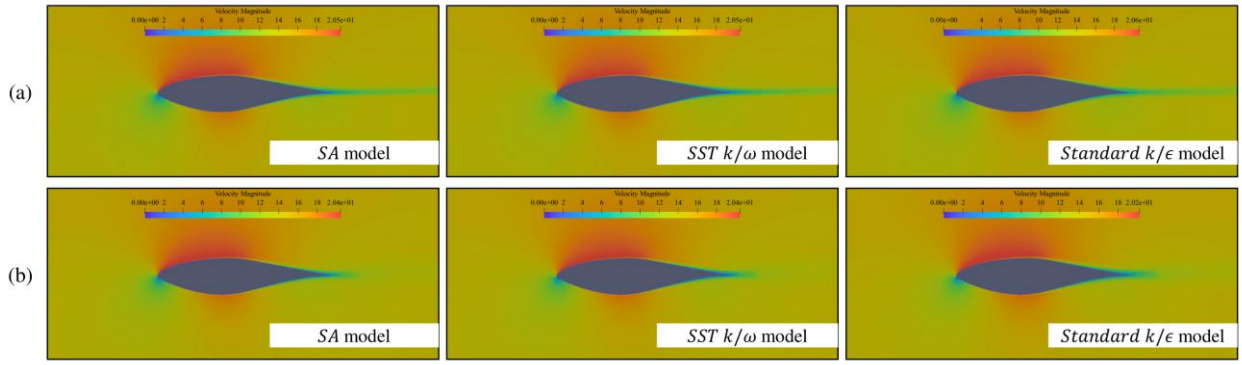

FIGURE 10. Contours of velocity at $\alpha = 4.10°$ at (a) structured mesh and (b) unstructured mesh for different turbulence models. Font: Authors (2022).

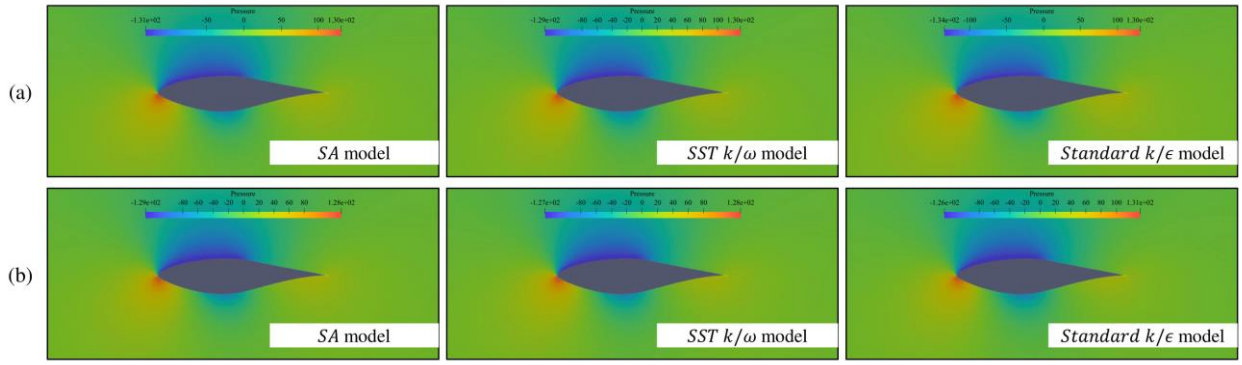

FIGURE 11. Contours of pressure at $\alpha = 4.10°$ at (a) structured mesh and (b) unstructured mesh for different turbulence models. Font: Authors (2022).

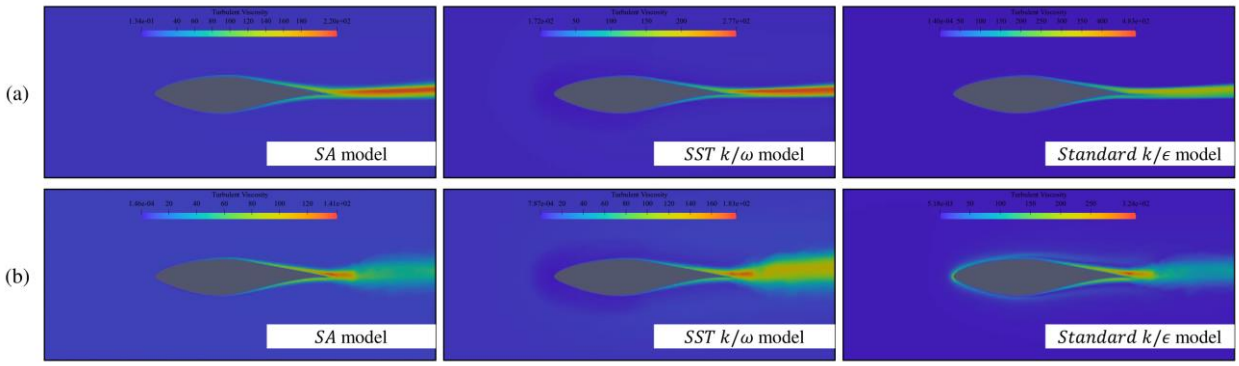

FIGURE 12. Contours of turbulence viscosity at $\alpha = 4.10°$ at (a) structured mesh and (b) unstructured mesh for different turbulence models. Font: Authors (2022).

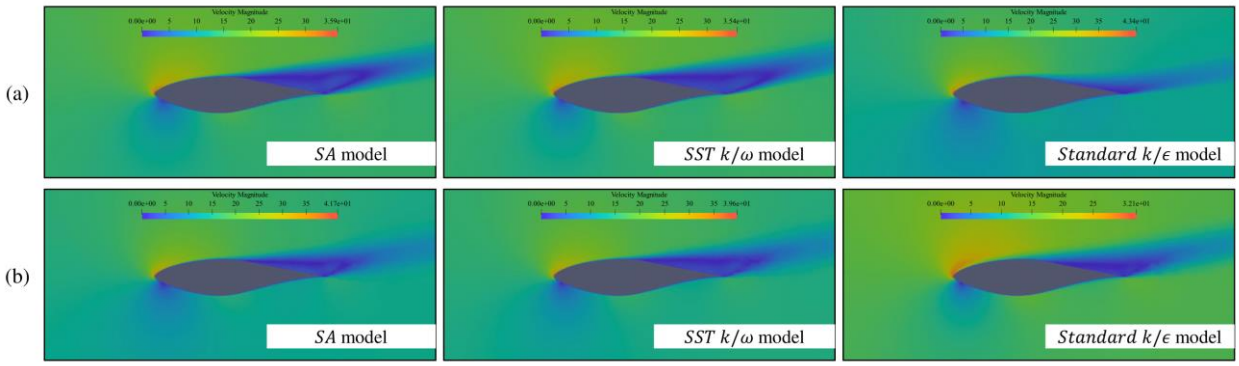

FIGURE 13. Contours of velocity at $\alpha = 15.23°$ at (a) structured mesh and (b) unstructured mesh for different turbulence models. Font: Authors (2022).

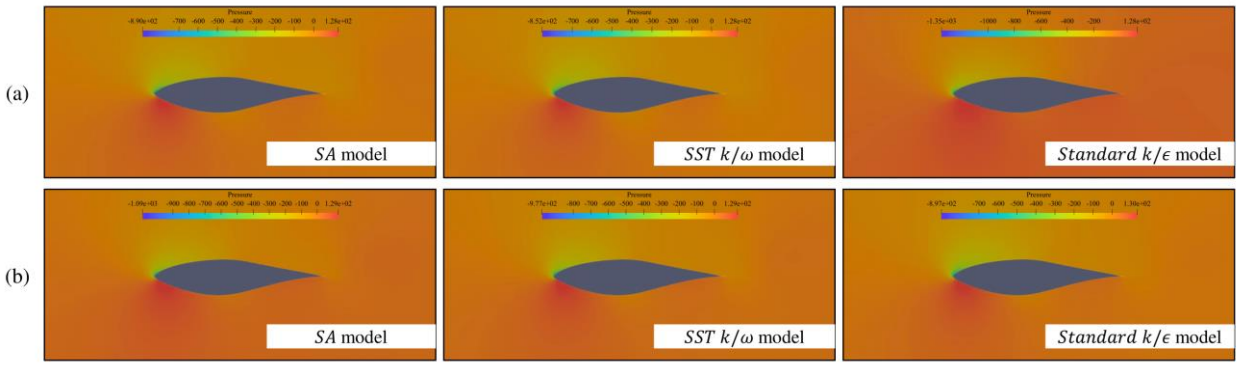

FIGURE 14. Contours of pressure at $\alpha = 15.23°$ at (a) structured mesh and (b) unstructured mesh for different turbulence models. Font: Authors (2022).

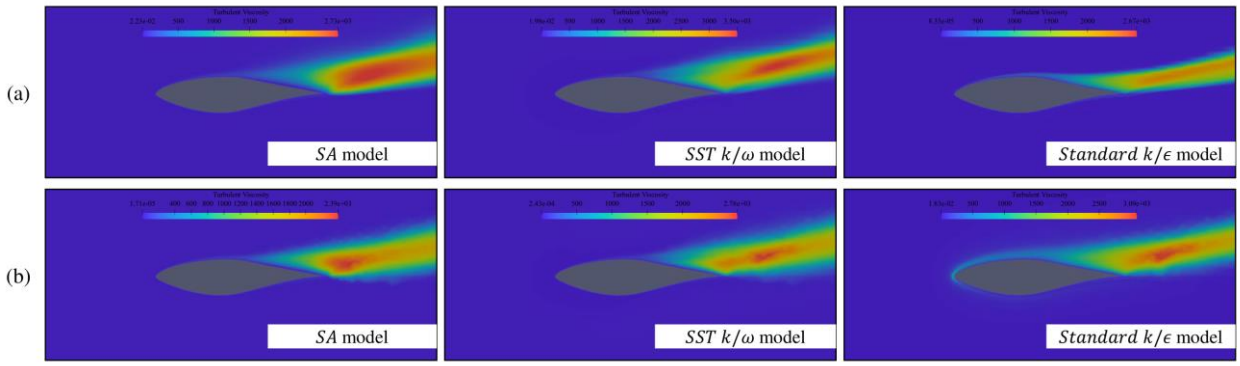

FIGURE 15. Contours of turbulence viscosity at $\alpha = 15.23°$ at (a) structured mesh and (b) unstructured mesh for different turbulence models. Font: Authors (2022).

We observed the consistency of the results through the velocity and pressure fields, for the different angles of attack, with a deceleration of the flow and an increase in pressure upstream of the aerodynamic profile. In addition, there is an acceleration of the flow along the surface of the profile, accompanied by a reduction in pressure. Note also the presence of the medium wake downstream of the profile. Through the turbulent viscosity fields, we observed that the region of greatest turbulent intensity modeled is in the wake region and on the airfoil surfaces. We also observed that the greater the turbulence in the slurry for higher angles of attack, expressed by the higher values of turbulent viscosity.

5. CONCLUSIONS

The results of the study indicate that the mesh dependency test is required to obtain accurate computational results. It was observed that the structured mesh is easier to solve and the computational cost is lower due to the number of cells compared to the unstructured mesh. For the structured mesh, at a cell number of 21000, the simulation results are already experiencing the convergence of the value of C_L and C_D by a less margin of error than unstructured mesh. With that result, the use of cell numbers up to 21000 with cells and $y^+ \cong 3$ is sufficient and is the optimum value to predict aerodynamic coefficients for an airfoil.

REFERENCES

Jonkman, J.M., 2003. “Modeling of the uae wind turbine for refinement of fast {_} ad”. Technical report, National Renewable Energy Lab., Golden, CO (US).

Fleck, G., Akwa, J. and Petry, A., 2014. “A computational study on the grid quality and convergence in 2d airfoils for small wind turbines”.

Salim, S.M. and Cheah, S., 2009. "Wall y+ strategy for dealing with wall-bounded turbulent flows". Vol. 2175.

Spalart, P.R. and Allmaras, S.R., 1992. "A one-equation turbulence model for aerodynamic flows". AIAA Paper. doi: doi.org/10.2514/6.1992-439. URL https://arc.aiaa.org/doi/10.2514/6.1992-439.

Çengel, Y.A. and Cimbala, J.M., 2010. Fluid Mechanics: Fundamentals and Applications. McGraw-Hill Higher Education.

Launder, B.E. and Spalding, D.B., 1972. Lectures in Mathematical Models of Turbulence. Academic Press.

Menter, F.R., Kuntz, M. and Langtry, R., 2003. "Ten years of industrial experience with the sst turbulence model". Turbulence, Heat and Mass Transfer, Vol. 4, pp. 625–632.

ACKNOWLEDGEMENTS

The authors would like to thank to Conselho Nacional de Desenvolvimento Científico e Tecnológico (CNPq) and the Federal University of Sao Joao del-Rei (UFSJ) for the support.